PNAS
www.pnas.org

Supplementary Information for:

Molecular mechanism of leukocidin GH - integrin CD11b/CD18 recognition and species specificity

Nikolina Trstenjak*, Dalibor Milić*, Melissa A. Graewert, Harald Rouha, Dmitri Svergun, Kristina Djinović-Carugo, Eszter Nagy, Adriana Badarau

Adriana Badarau

Email: adriana.badarau@x4pharma.com

This PDF file includes:

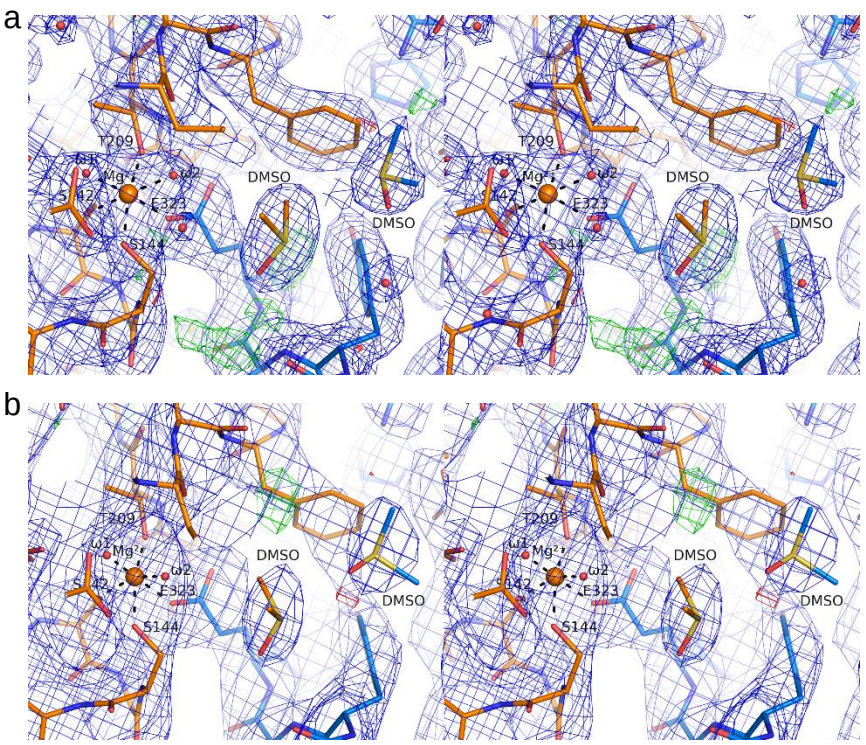

Supplementary Figure 1. Portion of electron density maps of the LukGH–CD11b-I complexes.

Stereo views of a portion of the electron density maps of **(a)** LukGH^{K319A}–moCD11b-I and **(b)** LukGH–huCD11b-I crystal structures. The σ_A-weighted $2mF_o–DF_c$ difference electron density maps contoured at 1.0σ level are shown as blue meshes. Contours at 3.0 and −3.0σ levels of the σ_A-weighted $mF_o–DF_c$ difference electron density maps are depicted as green and red meshes, respectively. LukH subunit is represented in blue and CD11b-I domain in orange. Mg^{2+} and water molecules are shown as orange and red spheres, respectively. Coordination of a Mg^{2+} cation is highlighted as dashed lines. Two putative DMSO molecules were modeled near the Mg^{2+} binding site at the LukH–CD11b-I interface.

a

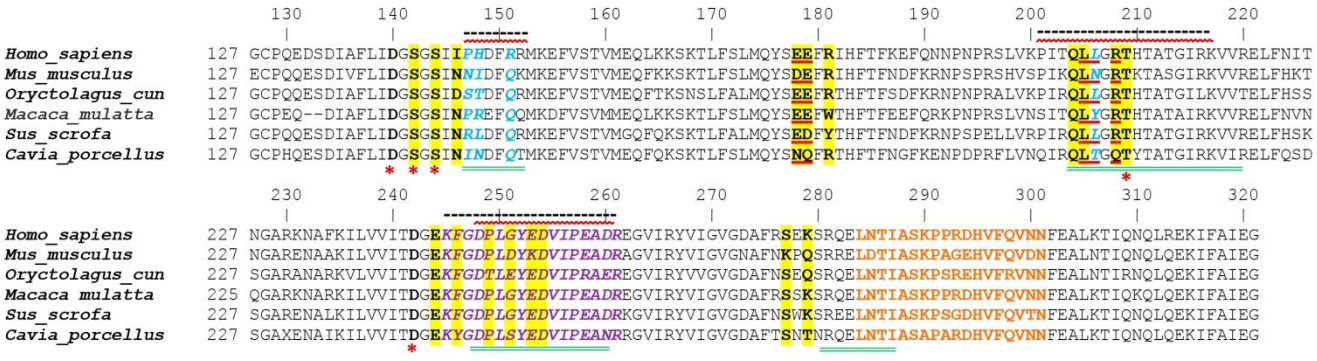

residues interacting with LukH and LukG, ***residues involved in metal coordination**, **C3d binding epitope (1)**, ***Human fibrinogen (Fg) binding epitope (2),*** iC3b binding epitope (3), NIF binding site (4), *C.albicans* hyphae binding epitope (5), **CBRM1/5 binding epitope (6)**, **LM2/1 binding epitope (7)**

b

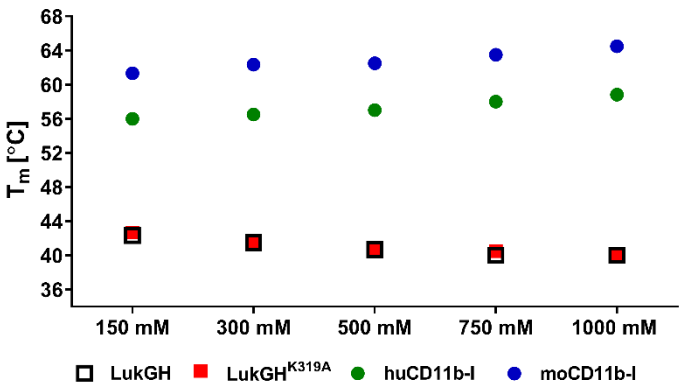

c

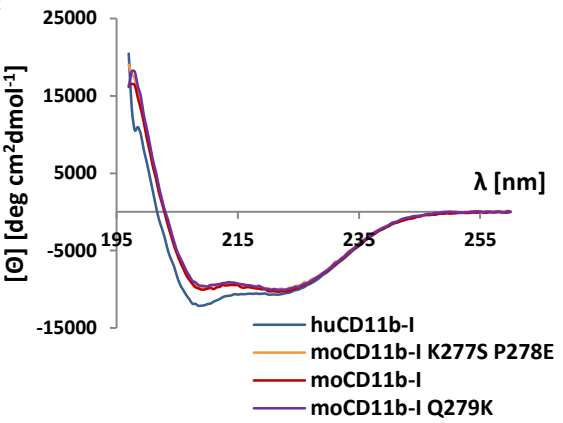

Supplementary Figure 2. Conservation of CD11b-I from different species and stability of CD11b-I variants.

(a) Alignment of CD11b-I residues 127–321 from different species.

(b) Melting temperature of LukGH, LukGH^{K319A} and CD11b-I variants, measured by DSF, in 25 mM HEPES, pH 7.5, 1 mM $MgCl_2$ with increasing NaCl concentrations (150–1000 mM).

(c) CD spectra of human, mouse CD11b-I and mouse CD11b-I variants in 50 mM sodium phosphate, pH 7.5, 300 mM NaCl.

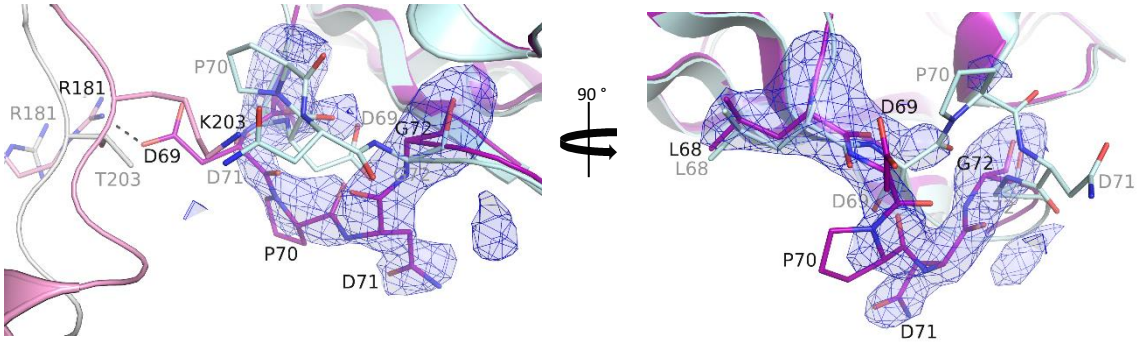

Supplementary Figure 3. Flexible loop in LukG.

The LukG loop 68–72 in the LukGH^{K319A}–moCD11b-I structure (purple) shows high flexibility and a different conformation from that found in the LukGH–huCD11b-I complex (light cyan). moCD11b-I is represented in pink and huCD11b-I in grey colour. The black residue labels correspond to the LukGH^{K319A}–moCD11b-I and the grey ones to the LukGH–huCD11b-I structure. The omit σ_A-weighted mF_o–DF_c difference electron density map contoured at 3.0σ level for LukGH^{K319A}–moCD11b-I is shown as a blue mesh. The salt bridge is highlighted as a dashed line.

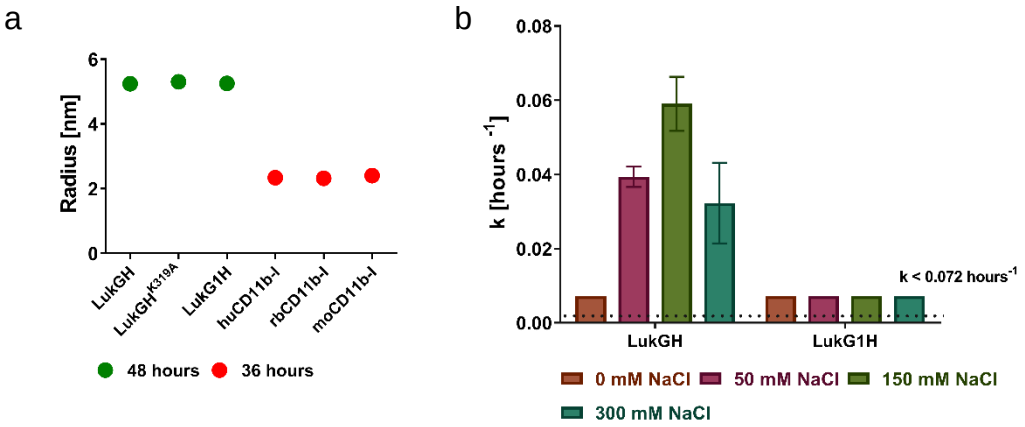

Supplementary Figure 4. Stability of LukGH variants and their oligomerisation in solution.

(a) Cumulant radius of individual LukGH mutants (at 5 mg/ml) and CD11b-I variants (at 2.5 mg/ml), measured by DLS, in 25 mM HEPES, pH 7.5, 1 mM $MgCl_2$, 150 mM NaCl after 48 or 36 h of incubation, respectively (one experiment with two replicates – some replicates are excluded due to poor autocorrelation curve) (mean of 1–2 replicates ± S.E.M).

(b) Oligomerization rate constant (k) for LukGH and LukG1H (at 5 mg/ml) in presence of rbCD11b-I (at 2.5 mg/ml) in 25 mM HEPES, pH 7.5, 1 mM $MgCl_2$, 0–300 mM NaCl (mean of 1–2 replicates ± S.E.M.). Data were fitted to a one-phase association model with fixed $y_0 = 5$ at $x_0 = 0$ h (GraphPad Prism), yielding $R^2 > 0.93$.

Supplementary Figure 5

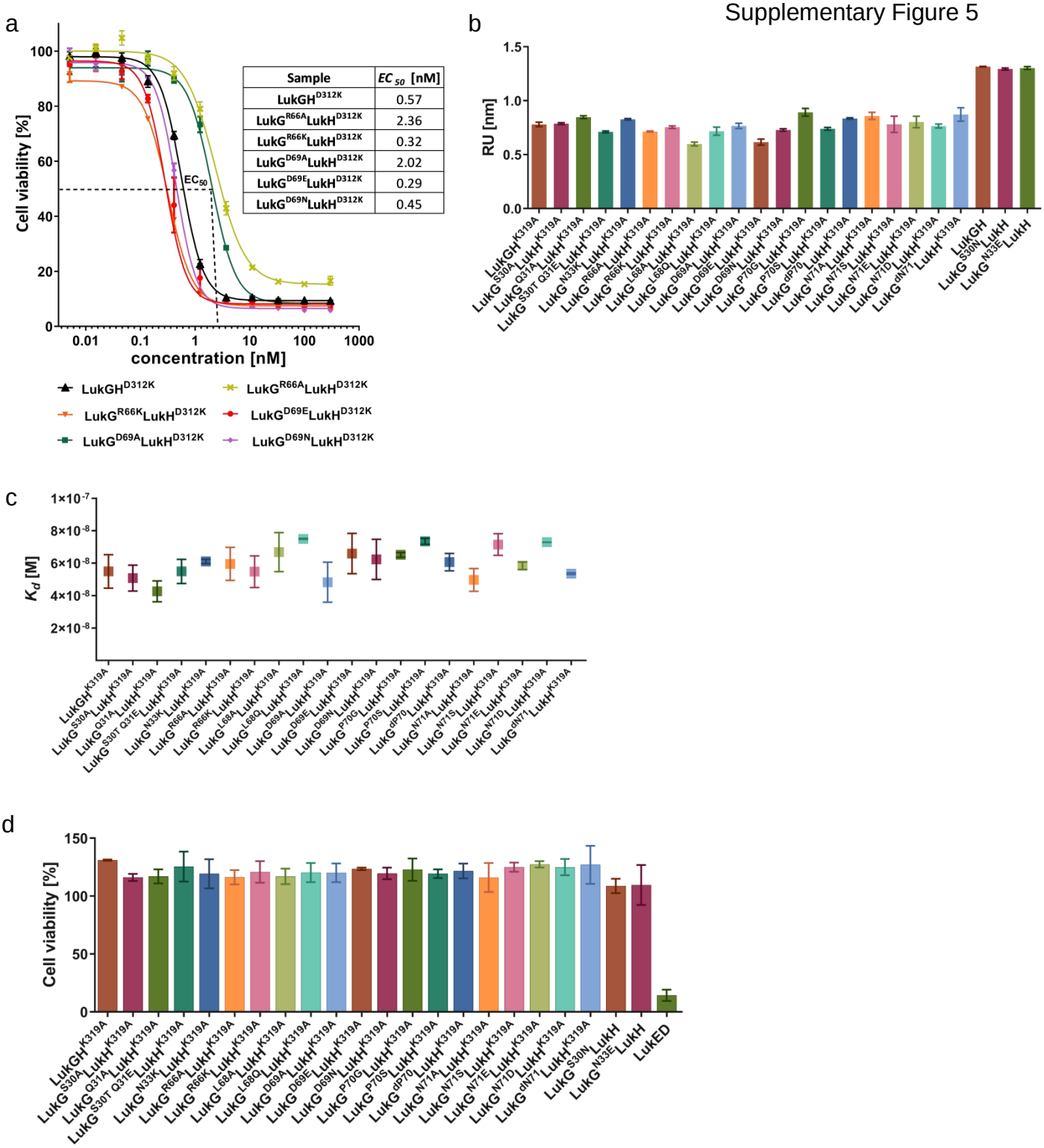

Supplementary Figure 5. Activity and receptor binding of LukGH oligomerization mutants.

(a) Activity of LukG oligomerization mutants (positions 66 and 69), co-expressed with LukH^{D312K}, towards rbPMNs assessed in a luminescent cell viability assay measuring cellular ATP content at increasing cytotoxin concentrations. Solid lines represent non-linear fit of the data and EC_{50} values are shown in the inserted table (mean of 3 replicates ± S.E.M.).

(b) Binding of LukGH oligomerization mutants in the LukH^{K319A} or LukH wild-type background (100 and 50 nM, respectively) to huCD11b-I, measured by BLI (mean of 2 independent experiments ± S.E.M). For the experiments with LukGH variants in the LukH wild-type background, the huCD11b-I was biotinylated with the amino specific reagent.

(c) Affinity of LukGH oligomerization mutants for moCD11b-I measured by BLI (mean of 2-4 independent experiments ± S.E.M.)

(d) Activity of LukGH variants towards mouse PMNs assessed in a luminescent cell viability assay measuring cellular ATP content at toxin concentration of 800–1000 nM for LukGH variants and 100 nM for LukED (mean of 2 independent experiments ± S.E.M).

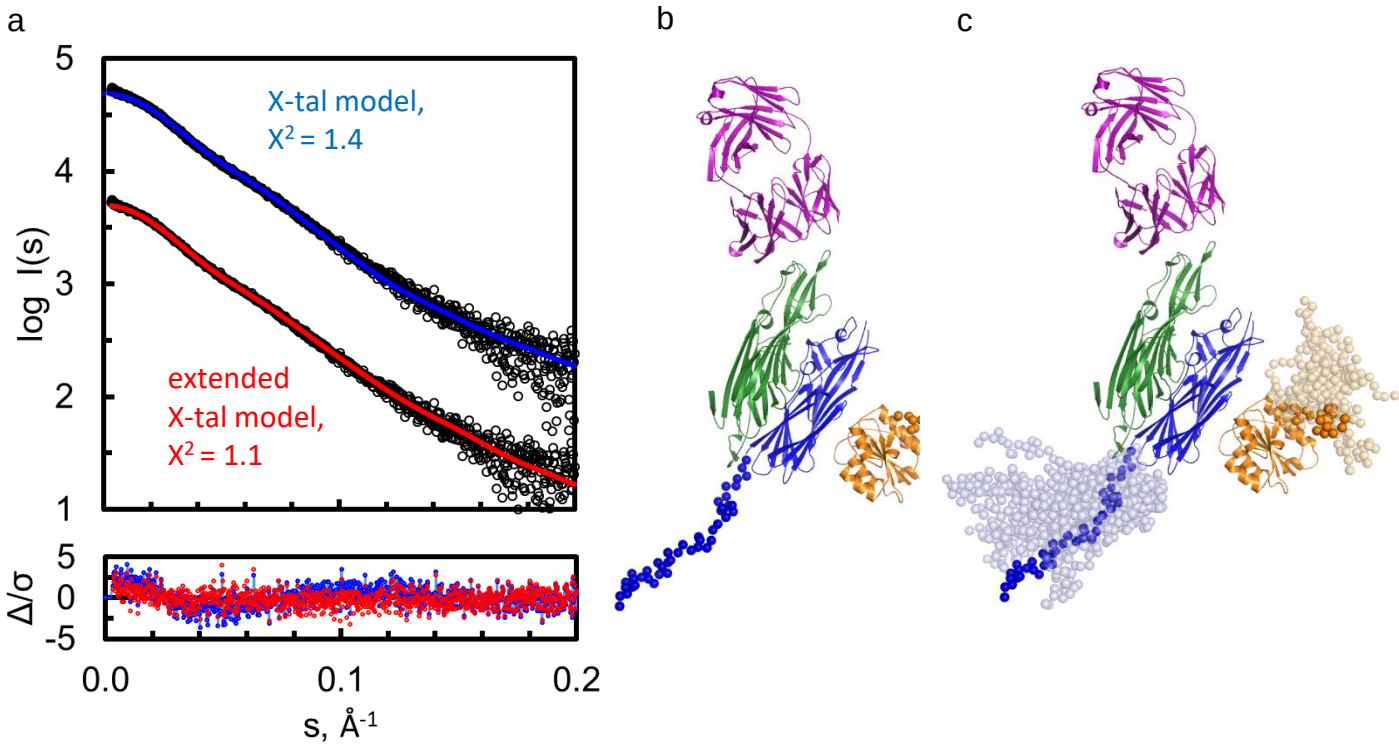

Supplementary Figure 6. SAXS data of FAB–LukGH–huCD11b-I complex and models obtained by CORAL.

(a) Fit and error-weighted residual difference plots of Fab–LukGH–huCD11b-I model with (red) and without (blue) extensions Data are shifted for clarity. X^2 values are indicated. The lower panel shows the residuals (Δ/σ) calculated as I_{exp} (s) – I_{model} (s) normalized with respect to experimental errors (σ).

(b) Representative model obtained with CORAL. Missing residues (44 residues from LukH N-terminus as well as 22 residues from huCD11b-I C-terminus) were modelled as dummy atoms to fit the experimental SAXS data and are shown as spheres. Color coding as in Figure 4.

(c) Overlay of 20 independent CORAL calculations. For clarity the model shown in B is emphasized.

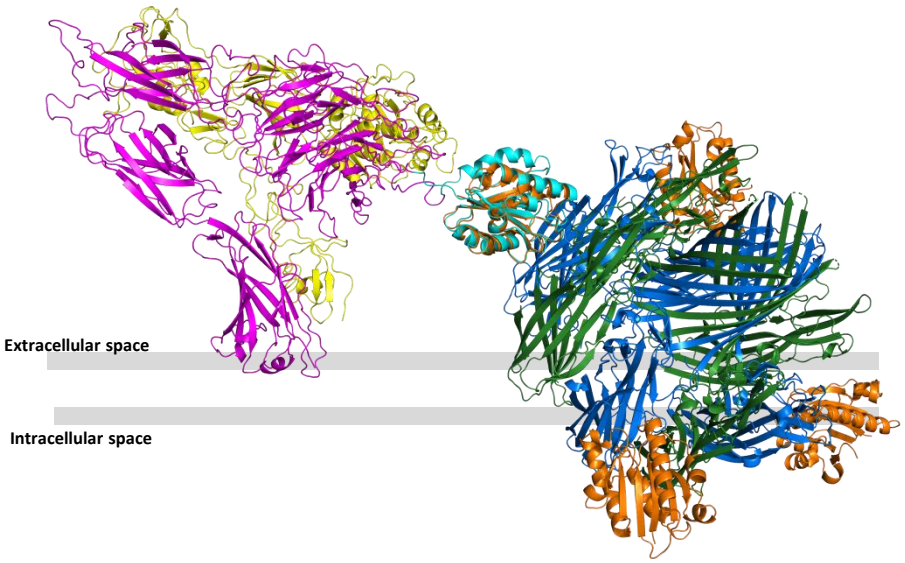

Supplementary Figure 7. Alignment of the LukGH^{K319A}–moCD11b-I complex with the CD11c/CD18 ectodomain.

(a) Alignment of the CD11b-I from LukGH^{K319A}–moCD11b-I crystal structure with CD11c-I domain of CD11c/CD18 (PDB 3K71). CD11c/CD18 (magenta and yellow cartoon, respectively, with CD11c-I domain as cyan cartoon) is in bent conformation, i.e. oriented towards the cellular membrane. LukG, LukH and CD11b-I are shown as green, blue and orange cartoon, respectively.

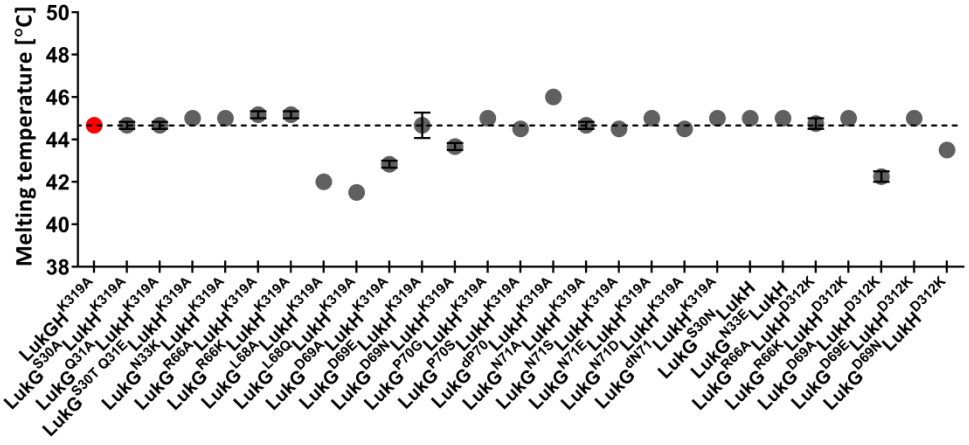

Supplementary Figure 8. Stability of LukGH variants

Melting temperature (T_m) of LukGH variants measured by DSF in 50 mM HEPES, pH 7.5 (mean of 2–3 replicates ± S.E.M). The T_m of LukGH^{K319A} is marked red.

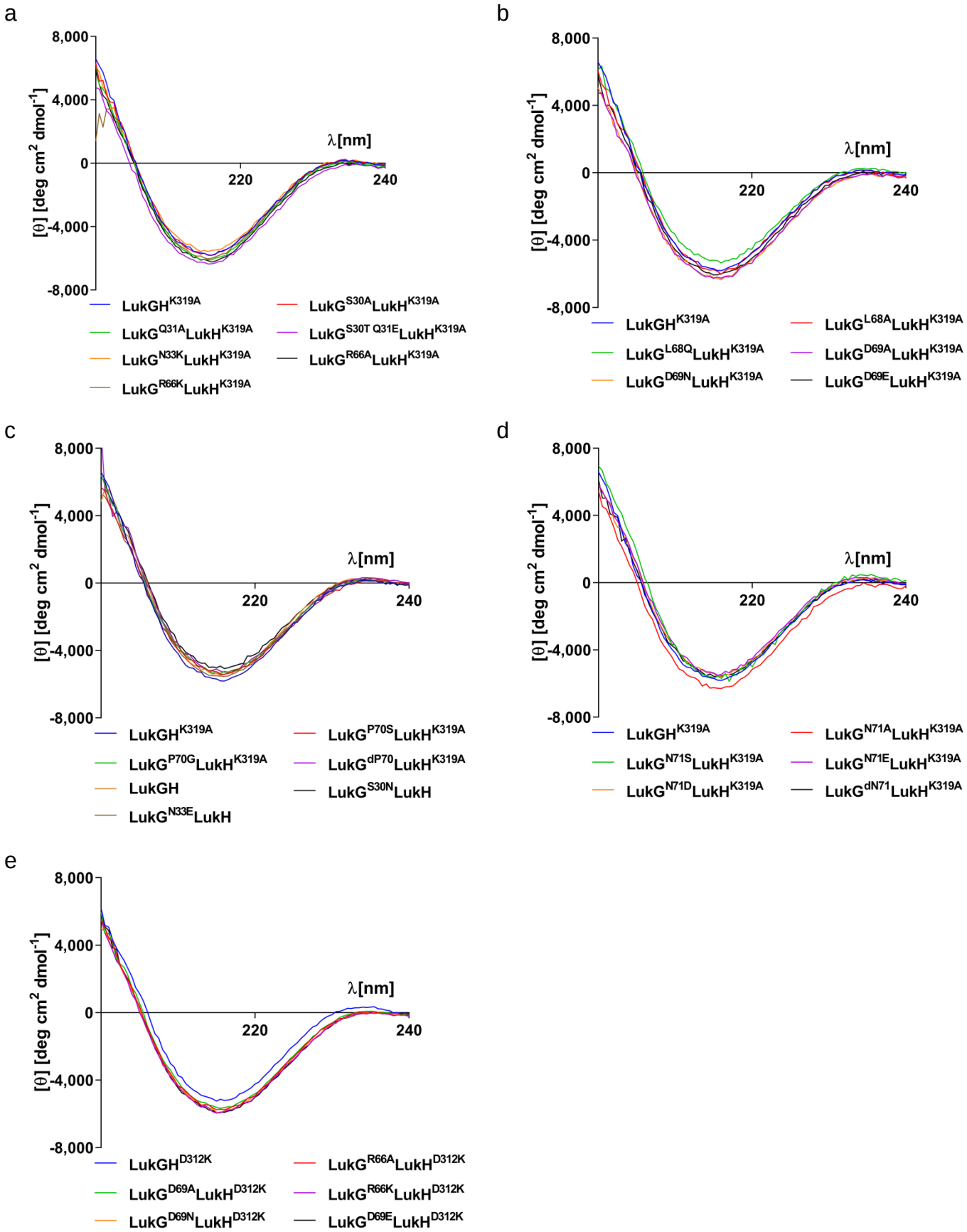

Supplementary Figure 9. Characterization of LukGH oligomerization mutants. (a) – (e) CD spectra of LukGH mutants in 20 mM sodium phosphate, pH 7.5, 150–250 mM NaCl.

a

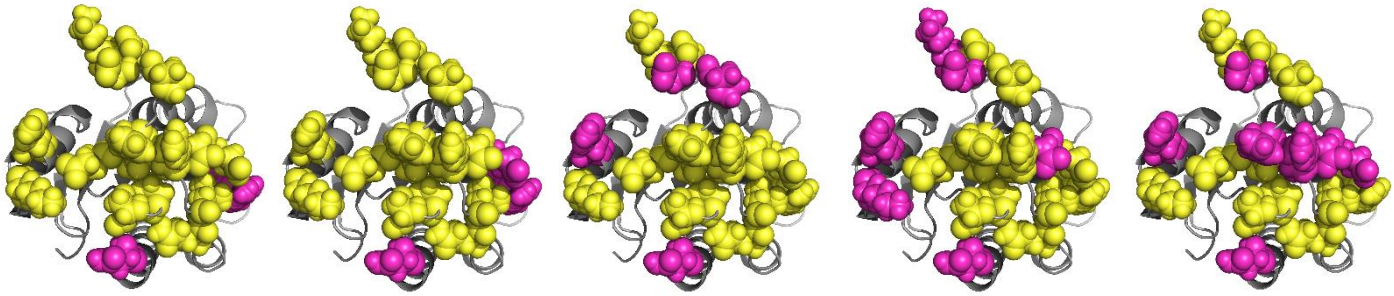

b

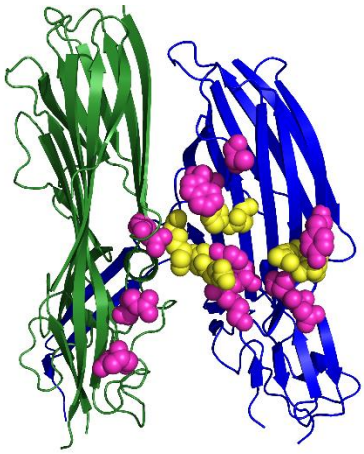

Supplementary Figure 10. Amino acid conservation of CD11b-I and LukGH residues from the binding epitope

(a) Amino acid conservation of the LukGH binding epitope in CD11b-I from rhesus macaque (*Macaca mulatta*), pig (*Sus scrofa*), rabbit (*Oryctolagus cuniculus)*, mouse (*Mus musculus*) and guinea pig (*Cavia porcellus*) CD11b-I compared to huCD11b-I is given as percentage (%) and displayed on the structure of moCD11b-I (grey cartoon). Conserved residues are shown as yellow and non-conserved as magenta spheres.

(b) Amino acid conservation of the LukGH residues involved in CD11b-I binding, among the LukGH sequence variants available in NCBI database (sequences with ≥ 90% coverage and ≥ 87% identity to TCH1516 sequence) displayed on the cartoon representation of the LukGH dimer (PDB 5K59, LukG in green and LukH in blue). Conserved residues are shown as yellow and non-conserved as magenta spheres.

SUPPLEMENTARY TABLES

Supplementary Table 1. Data collection, refinement and validation statistics.

	LukGH^{K319A}–moCD11b-I†	**LukGH–huCD11b-I‡**
Data collection		
Space group	$P42_12$	$P42_12$
Cell dimensions		
a, *b*, *c* (Å)	130.49, 130.49, 109.05	122.11, 122.11, 133.70
α, β, γ (°)	90, 90, 90	90, 90, 90
Resolution (Å)	46.94–2.29 (2.37–2.29)*	45.08–2.75 (2.99–2.75); anisotropic diffraction to 2.75 Å along **a*** and **b***, and 4.79 Å along **c***
R_{meas}	0.206 (2.566)	0.324 (1.739)
Mean $I/\sigma(I)$	7.5 (0.6)	7.8 (1.8)
Completeness (spherical, %)	99.3 (97.6)	53.8 (15.0)
Completeness (ellipsoidal, %)	99.3 (97.6)	92.0 (71.7)
Effective resolution (Å) [8]	2.30	3.38
Redundancy	5.6 (4.5)	12.6 (12.5)
$CC_{1/2}$	0.993 (0.212)	0.996 (0.627)
Refinement		
Resolution (Å)	46.94–2.29 (2.37–2.29)	45.08–2.75 (2.85–2.75)
No. reflections	42957 (4124)	14518
R_{work} / R_{free} (%)	18.8 (31.4)/22.7 (34.7)	23.9 (37.7)/28.1 (25.8)
No. non-H atoms		
Protein	6044	5730
Ligand/ion	25	25
Water	356	2
Average *B*-factors (Å^2)		
Protein	54.4	61.1
Ligand/ion	74.1	72.3
Water	49.1	28.3
R.m.s. deviations		
Bond lengths (Å)	0.002	0.003
Bond angles (°)	0.49	0.78
Ramachandran favoured (%)	94.7	94.6
Ramachandran outliers (%)	0.0	0.0

*Values in parentheses are for highest-resolution shell.
† Diffraction data were collected from one crystal.
‡Diffraction data were collected from one crystal that diffracted anisotropically to 2.75 Å along **a*** and **b***, and 4.79 Å along **c***.

Supplementary Table 2. Interacting residues between LukH and CD11b-I from LukGH–huCD11b-I and LukGH^{K319A}–moCD11b-I complexes. Conservation of LukH residues in LukH sequences in the three most divergent sequence variants of TCH1516 (MRSA252, MSHR and H19) and in sequence variants available in NCBI database (only the sequences with ≥90% coverage and ≥87% identity to TCH1516 sequence were analyzed).

LukGH^{K319A}–moCD11b-I		LukGH–huCD11b-I		Amino acid difference in sequence variants H19, MRSA252 or MSHR1132	Amino acids present in other sequence variants (% of sequences with position different from TCH1516)
LukH^{K319A}	moCD11b-I	LukH	huCD11b-I		
Residues involved in salt-bridge formation					
Gly 324 (C-terminus)	Arg 208	Gly 324 (C-terminus)	Arg 208	conserved	conserved
		Lys 319	Glu 244	Gln (MSHR1132)	Gln (3.6%)
Asp 316	Lys 277			conserved	conserved
Arg 294	Glu 244	Arg 294	Glu 244	conserved	conserved
Lys 183	Asp 178	Lys 183	Glu 178	conserved	conserved
Arg 119	Asp 251	Arg 119	Glu 253	conserved	Ser (7.2%)
Arg 119	Asp 254	Arg 119	Asp 254		
Residues involved in polar and hydrophobic contacts					
Glu 323#	Ser 144#	Glu 323#	Ser 144#	conserved	conserved
Glu 323*	Arg 208	Glu 323*	Arg 208		
Glu 323#	Thr 209#	Glu 323#	Thr 209#		
Glu 323#	Ser 142#	Glu 323#	Ser 142#		
Lys 322	Asn 146			Arg (MSHR1132)	Arg (23.7%)
Tyr 321	Arg 208, Phe 246	Tyr 321	Arg 208, Phe 246	Phe (MSHR1132)	Phe (23%)
Asn 318*	Lys 277			not present (MSHR1132)	not present (3.8%))
Asp 316	Lys 277	Asp 316	Ser 277	conserved	conserved
Tyr314	Gln279	Tyr 314	Ser 277	conserved	His (0.7%)
Arg 294	Glu 244	Arg 294	Glu 244	conserved	conserved
His 188	Arg 208, Phe 246	His 188	Arg 208, Phe 246	conserved	conserved
Trp 187	Pro 249	Trp 187	Pro 249	Arg (MRSA252)	Arg (10.1%)
Asp 114	Phe 246	Asp 114	Phe 246	conserved	conserved

* main chain O; # Mg^{2+}-coordinating residue

Supplementary Table 3. Binding of LukGH (50 nM) to huCD11b-I, measured by BLI, in buffers with different metals.

Buffer	RU (nm)	K_d (M)	k_{on} (M^{-1} s^{-1})	k_{dis} (s^{-1})
PBS + 1% BSA+ 1 mM $MgCl_2$	1.68	$1.2\times10^{-8} \pm 9.4\times10^{-11}$	$6.9\times10^{4} \pm 4.4\times10^{2}$	$7.9\times10^{-4} \pm 4.1\times10^{-6}$
PBS + 1% BSA+ 1 mM $MgCl_2$ + 1 mM $CaCl_2$	0.96	$2.4\times10^{-8} \pm 3.0\times10^{-10}$	$1.0\times10^{5} \pm 1.1\times10^{3}$	$2.4\times10^{-3} \pm 1.1\times10^{-5}$
PBS + 1% BSA+ 1 mM $CaCl_2$	0.02	/	/	/

*RU < 0.05 nm = no binding

Supplementary Table 4. Binding of LukGH or $LukGH^{K319A}$ to human or mouse CD11b-I in buffer (25 mM HEPES, pH 7.5, 1% BSA and 1 mM $MgCl_2$) with increasing salt concentration (150–1000 mM).

LukGH-huCD11b-I				
NaCl (mM)	**RU (nm)**	**K_d (M)**	**k_{on}(M^{-1} s^{-1})**	**k_{dis}(s^{-1})**
150	1.55 ± 0.18	$1.3\times10^{-8} \pm 7.8\times10^{-11}$	$1.3\times10^{5} \pm 2.0\times10^{4}$	$1.7\times10^{-3} \pm 2.5\times10^{-4}$
300	0.94 ± 0.04	$2.4\times10^{-8} \pm 7.5\times10^{-10}$	$1.4\times10^{5} \pm 2.0\times10^{4}$	$3.4\times10^{-3} \pm 3.8\times10^{-4}$
500	0.62 ± 0.08	$4.6\times10^{-8} \pm 4.5\times10^{-9}$	$1.2\times10^{5} \pm 1.2\times10^{3}$	$5.3\times10^{-3} \pm 5.8\times10^{-4}$
750	0.33 ± 0.05	$8.8\times10^{-8} \pm 5.8\times10^{-9}$	$8.6\times10^{4} \pm 4.1\times10^{2}$	$7.6\times10^{-3} \pm 4.6\times10^{-4}$
1000	0.22 ± 0.03	$1.3\times10^{-7} \pm 5.2\times10^{-9}$	$7.6\times10^{4} \pm 1.1\times10^{3}$	$9.5\times10^{-3} \pm 5.4\times10^{-4}$
$LukGH^{K319A}$–moCD11b-I				
150	0.66 ± 0.01	$5.3\times10^{-8} \pm 2.7\times10^{-9}$	$1.3\times10^{5} \pm 1.8\times10^{4}$	$6.7\times10^{-3} \pm 1.3\times10^{-3}$
300	0.28 ± 0.02	$1.1\times10^{-7} \pm 4.4\times10^{-9}$	$1.4\times10^{5} \pm 2.4\times10^{4}$	$1.5\times10^{-2} \pm 2.1\times10^{-3}$
500	0.13 ± 0.001	$1.4\times10^{-7} \pm 4.6\times10^{-8}$	$1.6\times10^{5} \pm 3.0\times10^{4}$	$2.2\times10^{-2} \pm 3.1\times10^{-3}$
750	0.06 ± 0.001*	/	/	/
1000	0.03 ± 0.001*	/	/	/

*RU < 0.05 nm = no binding

Supplementary Table 5. Interacting residues between LukG and CD11b-I from LukGH–huCD11b-I and LukGH^{K319A}–moCD11b-I complexes. Conservation of LukG residues in LukG sequences in the three most divergent sequence variants of TCH1516 (MRSA252, MSHR and H19) and in sequence variants available in NCBI database (only the sequences with≥ 90% coverage and ≥ 87% identity to TCH1516 sequence were analyzed).

LukGH^{K319A}–moCD11b-I		**LukGH–huCD11b-I**		**Amino acid difference in sequence variants H19, MRSA252 or MSHR1132**	**Amino acids present in other sequence variants (% of sequences with position different from TCH1516)**
LukG	**moCD11b-I**	**LukG**	**huCD11b-I**		
Residues involved in salt bridge formation					
Arg 66	Glu 179			Lys (MSHR1132, MRSA252)	Lys (20.5%)
Asp 69	Arg 181			Glu (H19), Asn (MRSA252)	Glu (13.7%), Asn (11%), Gly (0.7%)
Residues involved in polar and hydrophobic contacts					
Asn 33	Asp 178	Asn 33	Glu 178	Lys (MSHR1132, MRSA252)	Lys (20.5%), Ile (0.7%)
		Arg 66	Gln 204*	Lys (MSHR1132, MRSA252)	Lys (20.5%)
Arg 66	Leu 205*	Arg 66	Leu 205*		

* main chain O

Supplementary Table 6. Data collection and SAXS derived parameters for LukGH–Fab and LukGH–Fab-huCD11b-I complex.

Data collection parameters		
Radiation source	Petra III (DESY, Hamburg, Germany)	
beamline	EMBL P12	
Detector	Pilatus 2M	
Beam geometry (mm, FWHM)	0.12 × 0.20	
Wavelength (nm)	0.124	
Sample-detector distance (m)	3.1	
Momentum transfer *s* range (nm^{-1})	0.08 - 3.5	
Exposure time (s)	0.045	
Temperature (°C)	20	
Overall parameters	**LukGH–Fab**	**LukGH–Fab–huCD11b-I**
Concentration range (mg/ml)	0.4-4.6	0.4-4.7
R_g from Guinier approximation (nm)	4.7 ± 0.2	5.0 ± 0.2
R_g from PDDF (nm)	4.9 ± 0.1	5.2 ± 0.1
D_{max} (nm)	16 ± 1	18 ± 1
Molecular weight from forward scattering $I(0)$, (kDa)	91 ± 15	121 ± 20
Molecular weight from excluded volume (kDa)	110 ± 20	130 ± 20
Molecular weight from DATMOV, (kDa)	110 ± 20	120 ± 20
Molecular weight from volume of correlation (kDa)	90 ± 15	105 ± 20
Molecular weight from sequence (monomer, kDa)	122	143
Software employed		
Primary data reduction	SASFLOW	
Data processing	PRIMUS	
Calculation and comparison of scattering data	Crysol / Oligomer	
Addition of missing residues	CORAL	
SASBDB accession code	SASDF55	SASDF45

Supplementary Table 7. Ligands of CD11b and their affinities as reported in the literature.

Ligand	K_d (M)	Method used
Platelet factor 4 (PF4)	$1.3\times10^{-6} \pm 0.2\times10^{-6}$ (9)	BLI with immobilized PF4 and the I-domain in solution
Hookworm-derived Neutrophil adhesion inhibitor (NIF)	1) 1×10^{-9} (10) 2) $2.1\times10^{-9} \pm 0.5\times10^{-9}$ (4)	1) Binding of biotinylated NIF to CD11b immobilized on the plate 2) Binding of I^{125} labelled NIF to the I-domain expressed on HEK293 cells
Myelin basic protein (MBP)	Three binding events: K_{d1} and $K_{d2}=10^{-4}$, $K_{d3}=10^{-6}$ (11)	SPR with immobilized MBP and the active I-domain in solution
LL-37 (broad spectrum anti-microbial peptide)	1) $5.0\times10^{-6} \pm 0.9\times10^{-6}$ (not 1:1 kinetics so separated into three binding events: $K_{d1}=1\times10^{-6}$, K_{d2} and $K_{d3}=10–100\times10^{-6}$ (12)) 2) 4 binding events: $K_{d1}= 0.1–0.5\times10^{-6}$, K_{d2} and $K_{d3}=10–100\times10^{-6}$, $K_{d4}=0.01\times10^{-6}$ (12)	1) SPR with immobilized LL-37 2) BLI with immobilized I-domain and LL-37 in solution
Fibrinogen (Fg)	1) $2.2\times10^{-7} \pm 0.6\times10^{-7}$ (13) 2) $2x10^{-4}$ (14) 3) $2.5\times10^{-7} \pm 0.7\times10^{-7}$ (15)	1) Binding of ^{125}I labelled fibrinogen to the I-domain immobilized on the plate 2) SPR with the immobilized Fg and active I-domain in the solution 3) SPR with the immobilized Fg binding to CD11b-$I^{123-315}$
C3d	1) 4×10^{-7} (1) 2) 4.5×10^{-7} (1) 3) $1.5\times10^{-6} \pm 0.2\times10^{-6}$ (12)	1) SPR with immobilized C3d and I domain in solution 2) ITC 3) SPR with immobilized C3d and I domain in the solution
iC3b	1) 6×10^{-7} (1) 2) $10^{-7}–10^{-6}$ (1) 3) $4.6\times10^{-7} \pm 1.5\times10^{-7}$ (15) 4) $6.6\times10^{-7} \pm 3.0\times10^{-7}$ (15)	1) ITC 2) SPR with immobilized iC3b binding to I-domain 3) BLI with immobilized binding to CD11b-$I^{123-315}$ 4) SPR with immobilized iC3b binding to CD11b-I^{I316G}
Pleiotrophin (PNT) (cytokine and growth factor)	$1.2\times10^{-6} \pm 0.2\times10^{-6}$ / $3.9\times10^{-6} \pm 0.1\times10^{-6}$ (16)	BLI with PNT immobilized on the surface by two different methods and with active I-domain in the solution
CD54 (ICAM-1)	$2.2\times10^{-7} \pm 0.4\times10^{-7}$ (15)	SPR immobilized CD54 binding to CD11b-$I^{123-315}$

SPR: Surface plasmon resonance, BLI: bio-layer interferometry, ITC: isothermal titration calorimetry

SUPPLEMENTARY RESULTS AND DISCUSSION

The $RMSD_{C\alpha}$ values between the LukGH from the structures reported here and each of the two crystallographically-independent LukGH octamers in PDB 4TW1 (17) are 0.88 and 1.04 Å over 2247 and 2257 superimposed Cα atoms for the mouse complex, and 0.59 and 0.73 Å over 2167 and 2161 superimposed Cα atoms for the human complex, respectively.

To explain additionally observed features in difference electron density maps, we included six discrete molecules of dimethyl sulfoxide (DMSO) per an asymmetric unit of each structure. One DMSO moiety (DMSO2) is positioned in a hydrophobic pocket in the rim of LukG, occupied by either the side chain of M103 from the antibody Fab fragment of an anti-LukGH antibody (aLukGH-mAb#5.H1H2) in the Fab-LukGH complex (PDB 5K59) (18) or the side chain of LukG_N206 in one of the four chains from the LukGH octamer (PDB 4TW1), indicating a potential lipid binding site (Figure 1d). This pocket is ~15 Å away from the canonical phosphocholine binding pocket in other beta barrel pore forming toxins (19, 20), which is occupied in all known LukGH structures by the side chain of M178.

We wanted to confirm the involvement of the individual residues of LukGH in oligomerisation and activity, and subsequently engineer LukGH that can oligomerise upon binding to moCD11b-I. We therefore generated a series of variants (Ala, natural variants and amino acid deletions, mainly in the $LukH^{K319A}$ background) and measured their activity (reported as EC_{50} values or cell viability at a fixed cytotoxin concentration) towards differentiated granulocyte-like HL-60 cells and mouse neutrophils and also oligomerisation in presence of the recombinant receptors. All mutants were characterized by CD spectra and melting temperatures (T_m) to exclude false positive results due to protein instability (Supplementary Figures 8 and 9). The mutants tested had T_m values similar to the wild-type, except for the L68 and D69 variants (lower T_m of D69 variants probably due to loss of stabilizing interactions with the adjacent β-sheet (Figure 2c)). Oligomerisation of the $LukG^{N33E}LukH$ and $LukG^{S30N}LukH$ mutants could not be measured, as they showed increased aggregation when tested alone or in presence of human or mouse CD11b-I. Interestingly, the $LukG^{D69A}LukH^{K319A}$, $LukG^{D69N}LukH^{K319A}$, $LukG^{D69E}LukH^{K319A}$, $LukG^{L68Q}LukH^{K319A}$ and $LukG^{N71D}LukH^{K319A}$ variants, which tend to aggregate when incubated alone for up to 36 h at room temperature (Figure 3f), were stabilized in complex with both human and mouse CD11b-I (Figure 3e, 3f), as octamers or heterodimers, respectively.

The LukGH pore formation on resting cells is more enigmatic. The receptor density itself is only ~2-fold decreased compared to LPS-activated cells (21), so it is presumably the presence of the closed

conformation of the integrin I domain and the lack of clustering that limit activity. This scenario is likely less physiologically relevant at late infection time points, as the *S. aureus* extracellular components activate PMNs (21), but may become relevant at the onset of the infection. Interestingly, the killing curves are particularly flat on insensitive PMNs (i.e. little dependency of killing on LukGH concentration) (21), implying that LukGH concentration is not rate limiting in this process. In absence of any other stimuli, LukGH itself was shown to be able to prime PMNs (22). It is thus possible that at early stages of the infection, (and LukGH is one of the earliest expressed leukocidins (23)), LukGH promotes an outside-in signaling with conversion of the integrin I domain to an open form, with binding occurring directly to the bent conformer followed by pore insertion.

Although LukGH oligomerisation in solution is a good predictor of cytolytic activity, i.e. no activity against mouse cells and no oligomerisation with the mouse receptor, the smaller surface area of the oligomeric interface in the human compared with the mouse complex, as found in the crystal structures, appears counter-intuitive. It is therefore tempting to speculate that flexibility on the outskirts of the interface is needed to promote oligomerisation (kinetically). This aspect must be considered when attempting to improve oligomerisation of LukGH towards a certain species based on the current structures. On the other hand, improving binding appears a much easier endeavor. Interestingly, the sequence conservation map of the interface (both on LukGH and CD11b-I side) also predicts higher conservation for residues forming the core of the interface, and higher diversity towards the edges (Supplementary Figure 10). In addition, the contact residues are not conserved between other CD11b integrins (CD11a, CD11c and CD11d), which explains the specificity of LukGH towards CD11b.

SUPPLEMENTARY MATERIAL AND METHODS

Production of moCD11b-I variants and expression and purification of recombinant huCD11b-I, rbCD11b-I and moCD11b-I

MoCD11b-I variants were generated with QuikChange II XL Site-Directed Mutagenesis Kit (Agilent, according to the manufacturer instructions) using the *moCD11b-I*_pET24a as a template. All plasmids were transformed into *E. coli* TUNER DE3 cells and protein expression was induced at 20 °C for 20 hours with 0.4 mM IPTG. HuCD11b-I and rbCD11b-I were purified as described previously (17, 24). MoCD11b-I wild-type and variants were purified by cation exchange (HiTrap SP FF, GE Healthcare) followed by size exclusion (HiLoad Superdex 75 pg, GE Healthcare) chromatography. The CD11b-I proteins were treated

overnight with iodoacetamide (20 mM, Applichem) to alkylate the free cysteine and prevent dimer formation. Iodoacetamide was removed on PD-10 columns (GE Healthcare) equilibrated with 50 mM sodium phosphate, pH 7.5 plus 300 mM NaCl.

Biotinylated huCD11b-I and moCD11b-I were generated with using the sulfhydryl-reactive reagent EZ-Link BMCC-Biotin (Thermo Scientific), according to the manufacturer's instructions. For moCD11b-I (in Figure 1b), the amino reactive reagent Sulfo-NHS-LC biotin (Thermo Scientific) was used, yielding final biotin/protein ratios of 0.3.

Circular dichroism (CD) and differential scanning fluorimetry (DSF) analysis

Far UV (195-250 nm) CD spectra of samples were recorded on a Chirascan (Applied Photophysics) spectrometer in a 0.5 mm cuvette (Applied Photophysics) at 20°C. The LukGH and CD11b-I samples were measured at concentrations of 0.2–1.0 mg/mL or 0.25–0.66 mg/mL, respectively, in 20 mM sodium phosphate, pH 7.5 plus 150–300 mM NaCl or 50 mM sodium phosphate, pH 7.5 plus 300 mM NaCl, respectively. The melting points (T_m) of the proteins were determined by differential scanning fluorimetry. The proteins were mixed with Sypro Orange dye and with corresponding buffer (either with HEPES, pH 7.5 (50 mM final concentration) or HEPES, pH 7.5 plus $MgCl_2$ (25 mM and 1 mM final concentration, respectively) and NaCl (150–1000 mM)). The assay was conducted in a qPCR instrument (Bio-Rad CFX96) and the T_m values determined using the Bio-Rad CFX Manager software.

Purification of LukGH–huCD11b-I–Fab and LukGH–Fab complexes and small angle X-ray scattering (SAXS) analysis

The LukGH-Fab and LukGH-Fab-huCD11b-I complexes were concentrated to approximately 10 mg/ml and purified on size exclusion chromatography (HiLoad Superdex 200 pg, GE Healthcare) equilibrated in 20 mM HEPES, pH 7.5, 300 mM NaCl, 1 mM $MgCl_2$. The LukGH–Fab–huCD11b-I and LukGH–Fab complexes were concentrated to 4.2 mg/mL and 4.6 mg/ml, respectively. Purity was assessed on non-reducing SDS-PAGE gel and polydispersity by dynamic light scattering (DLS). Synchrotron radiation X-ray scattering images were recorded using a photon counting Pilatus-2M detector at a sample to detector distance of 3.1 m and a wavelength (λ) of 0.12 nm covering the range of momentum transfer $0.08 < s < 3.5$ nm^{-1} ($s = 4\pi \sin\vartheta/\lambda$, where 2ϑ is the scattering angle). A continuous flow cell capillary was used to reduce radiation damage. The latter was monitored by collecting 20 successive 50 ms exposures, comparing the frames, and discarding those displaying significant alterations. Data reduction to produce the final scattering profiles of the complexes were performed using standard methods. Briefly, for 2D-

to-1D radial averaging the SASFLOW pipeline was used (25). Scattering profiles from the buffer without protein were used for background subtraction.

To exclude any dissociation process, the program OLIGOMER (26) was used to check if the fits could be improved by additionally allowing some volume fractions of the individual subunits. This was not the case.

To account for missing residues not resolved in the crystal structure the program CORAL (27) was used. Here, additional beads representing the individual residues are added to the available crystal structures to optimize the fit to the experimental SAXS data. 44 beads were added to the N-terminus of LukH and 22 residues to the C-terminus of huCD11b-I. 20 independent calculations were performed and the models obtained were compared to each other.

Dynamic light scattering (DLS) and oligomerisation assay

LukGH, CD11b-I and Fab αLukGH-mAb#5.H1H2 were dialyzed separately against 25 mM HEPES, pH 7.5 plus 1 mM $MgCl_2$ and concentrated to final concentrations of 1–5 mg/ml for LukGH, 0.5–2.5 mg/ml for CD11b-I and 1 mg/ml for Fab αLukGH-mAb#5.H1H2. After addition of NaCl (0–300 mM) to the samples, LukGH and CD11b-I were mixed either in fixed (1:1 for huCD11b-I, 1:1.2 for moCD11b-I and 1:1.4 for rbCD11b-I) or in variable (1:0.1 – 1:1 for huCD11b-I) ratios. For the experiments with the aLukGH-mAb#5.H1H2 Fab, the ratios were 1:1.5, 1.5:1 and 1:1:1.5 for LukGH:Fab, Fab:huCD11b-I and LukGH:huCD11b-I:Fab, respectively. The samples were spin filtered (Ultrafree MC, 0.1 µM, Merck) before the measurements. Duplicates of each sample were transferred into a 1536 Microplate with glass bottom (Greiner) and covered with silicone oil. Scattering data were collected at pre-set time points. The calculated autocorrelation function was analyzed by cumulant fit, assuming one population of particles with a single average diffusion coefficient and a single standard deviation about that average, using DYNAMICS 7.7.0.125 software (Wyatt Technology). The data with low intensity, or poor fits with the baseline >1.01 and the sum-of-squares error (*SOS*) > 10 were excluded from further analysis.

Cytotoxicity assay

The HL-60 cells (ATCC® CCL-240™) were differentiated into granulocyte-like cells using dimethylformamide (DMF) as described previously (24). Human PMNs were isolated from heparinized human whole blood, obtained from healthy volunteers, using Percoll® (Percoll Plus, GE Healthcare) gradient centrifugation as described previously (17). Rabbit PMNs were isolated from rabbit whole blood (New Zealand White rabbits) anti-coagulated with citrate dextrose solution, using Histopaque 1077 (Sigma-Aldrich) and HetaSep (Stemcell Technologies) as described previously (28). Mouse PMNs were purified from mouse whole blood with acid-citrate-dextrose anti-coagulant (ACD), obtained from BALB/C mice, using EasySep™ Mouse Neutrophil Enrichment Kit (Stemcell Technologies), according to manufacturer's instruction. Human, rabbit (both at $2.5x10^4$ cells/well) or mouse PMNs ($1x10^4$ – $2.5x10^4$ cells/well) were exposed to LukGH (serial dilutions (0.002 to 100 nM for human and 0.005 to 300 nM for rabbit cells) or fixed concentration (800 nM, 1000 nM, 20 µM, 30 µM for mouse PMNs)) or LukED (0.002 to 100 nM) in assay medium (RPMI plus 10% FBS and L-Glutamine) at 37 °C, 5% CO_2 for 4 h.

Purification of protein complexes for crystallization

$LukGH^{K319A}$ with moCD11b-I or LukGH wild-type with huCD11b-I (all proteins were purified as described in Material and Methods and SI Material and Methods) were mixed in 1:1.2 and 1:1 molar ratio, respectively, after dialyzing the individual proteins in 25 mM HEPES, pH 7.5. The mixtures were concentrated, and the complexes purified on a cation exchange column (SP FF, GE Healthcare) equilibrated in 20 mM sodium phosphate, pH 7.5, 50 mM NaCl plus 1 mM $MgCl_2$ using a 0–0.95 M linear gradient of NaCl in the same buffer. The complexes eluted at ~300 mM NaCl and fractions containing both proteins, based on the SDS-PAGE gel, were combined and buffer exchanged (PD-10 column, GE Healthcare) into 25 mM HEPES, pH 7.5 plus 1 mM $MgCl_2$ (and 50 mM NaCl for the mouse complex).

SUPPLEMENTARY REFERENCES:

1. G. Bajic, L. Yatime, R. B. Sim, T. Vorup-Jensen, G. R. Andersen, Structural insight on the recognition of surface-bound opsonins by the integrin I domain of complement receptor 3. *Proc. Natl. Acad. Sci. U.S.A.* **110,** 16426–16431 (2013).

2. V. P. Yakubenko, V. K. Lishko, S. C. T. Lam, T. P. Ugarova, A molecular basis for integrin $\alpha_M\beta_2$ Ligand binding promiscuity. *J. Biol. Chem.* **277**, 48635–48642 (2002).

3. L. Zhang, E. F. Plow, Amino acid sequences within the α subunit of integrin $\alpha_M\beta_2$ (Mac-1) critical for specific recognition of C3bi. *Biochemistry* **38**, 8064–8071 (1999).

4. L. Zhang, E. F. Plow, Identification and reconstruction of the binding site within $\alpha_M\beta_2$ for a specific and high affinity ligand, NIF. *J. Biol. Chem.* **272,** 17558–17564 (1997).

5. C. B. Forsyth, E. F. Plow, L. Zhang, Interaction of the fungal pathogen *Candida albicans* with integrin CD11b/CD18: Recognition by the I domain is modulated by the lectin-like domain and the CD18 subunit. *J. Immunol.* **161**, 6198-6205 (1998).

6. C. Oxvig, C. Lu, T. A. Springer, Conformational changes in tertiary structure near the ligand binding site of an integrin I domain. *Proc. Natl. Acad. Sci. U.S.A.* **96,** 2215–2220 (1999).

7. S. M. Violette, J. R. Rusche, S. R. Purdy, J. G. Boyd, J. Cos, Differences in the binding of blocking anti-CD11b monoclonal antibodies to the A-domain of CD11b. *J. Immunol.* **155**, 3092-3101 (1995).

8. M. Weiss, Global indicators of X-ray data quality. J. Appl. Crystallogr. **34**(2),130-135 (2001).

9. V. K. Lishko, V. P.Yakubenko, T. P. Ugarova, N. P. Podolnikova, Leukocyte integrin Mac-1 (CD11b/CD18, $\alpha_M\beta_2$, CR3) acts as a functional receptor for platelet factor 4. *J. Biol. Chem.* **293**, 6869–6882 (2018).

10. P. Rieu, T. Ueda, I. Haruta, C. E. Sharma, M. A. Arnaout, The A-Domain of β2 integrin CR3 (CDllb/CD18) is a receptor for the hookworm-derived neutrophil adhesion inhibitor NIF. *J. Cell Biol.* **127**, 11 (1994).

11. R. Stapulionis, C. L. Oliveira, M. C. Gjelstrup, J. S. Pedersen, M. E. Hokland *et al*., Structural insight into the function of myelin basic protein as a ligand for integrin $\alpha_M\beta_2$. *J. Immunol.* **180**, 3946–3956 (2008).

12. X. Zhang, G. Bajic, G. R. Andersen, S. H. Christiansen, T. Vorup-Jensen, The cationic peptide LL-37 binds Mac-1 (CD11b/CD18) with a low dissociation rate and promotes phagocytosis. *Biochim. Biophys. Acta* **1864**, 471–478 (2016).

13. L. Zhou, D. H. S. Lee, J. Plescia, C. Y. Lau, D. C. Altieri, Differential ligand binding specificities of recombinant CDllb/CD18 integrin I-domain. *J. Biol. Chem.* **269**, 17075-17079 (1994).

14. T. Vorup-Jensen, C. V. Carman, M. Shimaoka, P. Schuck, J. Svitel *et al*., Exposure of acidic residues as a danger signal for recognition of fibrinogen and other macromolecules by integrin αXβ2. *Proc. Natl. Acad. Sci. U.S.A.* **102**, 1614–1619 (2005).

15. J. P. Xiong, R. Li, M. Essafi, T. Stehle, M. A. Arnaout, An isoleucine-based allosteric switch controls affinity and shape shifting in integrin CD11b A-domain. *J. Biol. Chem.* **275**, 38762–38767 (2000).

16. D. Shen, N. P. Podolnikova, V. P. Yakubenko, C. L. Ardell, A. Balabiyev *et al*., Pleiotrophin, a multifunctional cytokine and growth factor, induces leukocyte responses through the integrin Mac-1. *J. Biol. Chem.* **292,** 18848–18861 (2017).

17. A. Badarau, H. Rouha, S. Malafa, D. T. Logan, M. Håkansson *et al*., Structure-function analysis of heterodimer formation, oligomerization, and receptor binding of the *Staphylococcus aureus* bi-component toxin LukGH. *J. Biol. Chem.* **290**, 142–156 (2015).

18. A. Badarau, H. Rouha, S. Malafa, M. B. Battles, L. Walker *et al.*, Context matters: The importance of dimerization-induced conformation of the LukGH leukocidin of *Staphylococcus aureus* for the generation of neutralizing antibodies. *mAbs* **8**, 1347–1360 (2016).

19. S. Galdiero, E. Gouaux, High resolution crystallographic studies of α-hemolysin-phospholipid complexes define heptamer-lipid head group interactions: Implication for understanding protein-lipid interactions. *Protein Sci.* **13**, 1503–1511 (2004).

20. Y. Tanaka, N. Hirano, J. Kaneko, Y. Kamio, M. Yao *et al*., 2-Methyl-2,4-pentanediol induces spontaneous assembly of staphylococcal α-hemolysin into heptameric pore structure. *Protein Sci.* **20**, 448–456 (2011).

21. P. Janesch, H. Rouha, S. Weber, S. Malafa, K. Gross *et al*., Selective sensitization of human neutrophils to LukGH mediated cytotoxicity by *Staphylococcus aureus* and IL-8. *J. Infect.* **74**, 473–483 (2017).

22. N. Malachowa, S. D. Kobayashi, B. Freedman, D. W. Dorward, F. R. DeLeo, *Staphylococcus aureus* leukotoxin GH promotes formation of neutrophil extracellular traps. *J. Immunol.* **191**, 6022–6029 (2013).

23. A. L. DuMont, P. Yoong, C. J. Day, F. 3rd Alonzo, W. H. McDonald *et al*., *Staphylococcus aureus* LukAB cytotoxin kills human neutrophils by targeting the CD11b subunit of the integrin Mac-1. *Proc. Natl. Acad. Sci. U.S.A.* **110**, 10794–10799 (2013).

24. N. Trstenjak, L. Stulik, H. Rouha, J. Zmajkovic, M. Zerbs *et al*., Adaptation of the *Staphylococcus aureus* leukocidin LukGH for the rabbit host by protein engineering. *Biochem. J.* **476**, 275-292 (2019).

25. D. Franke, M. V. Petoukhov, P. V. Konarev, A. Panjkovich, A. Tuukkanen *et al*., *ATSAS 2.8*: a comprehensive data analysis suite for small-angle scattering from macromolecular solutions. *J. Appl. Crystallogr.* **50**, 1212–1225 (2017).

26. P. V. Konarev, V. V. Volkov, A. V. Sokolova, M. H. J. Koch, D. I. Svergun, *PRIMUS* : a Windows PC-based system for small-angle scattering data analysis. *J. Appl. Crystallogr.* **36**, 1277–1282 (2003).

27. M. V. Petoukhov, D. Franke, A. V. Shkumatov, G. Tria, A. G. Kikhney *et al*., New developments in the ATSAS program package for small-angle scattering data analysis. *J. Appl. Crystallogr.* **45**, 342–350 (2012).

28. D. W. Siemsen, N. Malachowa, I. A. Schepetkin, A. R. Whitney, L. N. Kirpotina *et al.*, “Neutrophil isolation from nonhuman species” in Neutrophil Methods and Protocols, M. T. Quin, F. R. DeLeo, Eds. (Humana Press, 2014), pp 19–37.